RSC Advances

PAPER

View Article Online
View Journal | View Issue

Cite this: *RSC Adv.*, 2026, **16**, 3753

Experimental study on the thermal conductivity of graphene–carbon nanotube–silver nanoparticle ternary hybrid nanofluids

Pham Van Trinh, *[ab] Nguyen Ngoc Anh,[a] Mai Thi Phuong,[a] Nguyen Van Tu,[a] Tran Van Hau, [a] Do Tuan,[a] Nguyen Thi Huyen,[a] Cao Thi Thanh,[a] Nguyen Van Hao, [c] Mone Phommahaxay,[c] Nguyen Thi Ngoc Mai,[c] Phan Ngoc Hong,[d] Phan Ngoc Minh,[b] Bui Hung Thang*[a] and Nguyen Van Chuc *[a]

In this study, high-thermal-conductivity ternary hybrid nanofluids incorporating graphene–carbon nanotube–silver (Gr–CNT–AgNP) hybrid materials were successfully prepared. The influence of nanoparticle concentration (0–0.05 vol%) and operating temperature (30–55 °C) on the thermal conductivity of both water-based and ethylene-glycol (EG)-based nanofluids was systematically examined. The thermal conductivity increased monotonically with Gr–CNT–AgNP loading, achieving maximum enhancements of 38% for water-based and 52% for EG-based nanofluids at 0.05 vol% and 55 °C. Quantitative analysis showed that concentration contributed more strongly to conductivity improvement than temperature, though temperature-induced intensification of Brownian motion provided an additional enhancement of up to ~10% across the tested range. A predictive thermal conductivity model was also developed, yielding an excellent fit to experimental data with deviations below 5%, thereby validating its accuracy and applicability. Overall, the Gr–CNT–AgNP ternary hybrid nanofluids demonstrate substantial potential for high-performance thermal management systems, including cooling, heat-transfer devices, and solar-thermal collectors.

Received 28th May 2025
Accepted 11th January 2026

DOI: 10.1039/d5ra03763h

rsc.li/rsc-advances

1 Introduction

Nanofluids have emerged as a promising class of advanced heat-transfer materials, consisting of a base fluid—typically deionized (DI) water or ethylene glycol (EG)—dispersed with nanoscale solid particles.[1,2] Their thermophysical behavior, particularly thermal conductivity, is strongly influenced by the physicochemical characteristics of the dispersed nanomaterials, including particle size, shape, and intrinsic thermal properties.[3,4] A wide range of nanomaterials such as Cu, Ag, CuO, Ni, Al_2O_3, and TiO_2 have been utilized to enhance the heat-transfer performance of conventional working fluids, primarily due to their high surface-to-volume ratios which facilitate more efficient interfacial heat exchange.[5–9] Since the discovery of carbon nanomaterials such as carbon nanotubes (CNTs) and graphene (Gr), significant research attention has shifted toward nanofluids incorporating carbon-based additives and their hybrid structures. These materials possess exceptional thermal, mechanical, and electrical properties that make them highly attractive for thermal management applications.[10,11] For instance, Hussein *et al.* reported that TiO_2/MWCNT nanofluids improved the thermal and rheological performance of flat-plate solar collectors, resulting in an efficiency enhancement of up to 84%.[10] Esfe *et al.*[12] demonstrated that hybrid MWCNT–MgO nanofluids achieved substantial improvements in thermal conductivity, while Sadri *et al.*[13] observed a 22.31% increase at 40 °C in nanofluids containing 0.5 wt% CNTs. Moreover, Yarmand and coworkers showed that Ag–Gr nanofluids at 0.1 wt% delivered a 22.22% enhancement at 40 °C.[14] Comparative studies have also highlighted that EG-based nanofluids generally outperform those based on DI water; for example, Aravind *et al.* reported thermal conductivity enhancements of 13.7% in EG *versus* 10.5% in DI water at the same volume fraction (0.04 vol%) of graphene–MWCNT additives.[15] Comprehensive reviews further confirm that the superior thermal conductivity of carbon nanomaterials is a primary driver of the enhancement observed in carbon-based nanofluids.[16] Building on this progress, recent research has expanded beyond mono- and binary nanofluids to explore ternary hybrid nanofluids (THFs), which incorporate three distinct nanoadditives into a base fluid.[17–19] THFs have attracted growing interest due to their potential to

[a]*Institute of Materials Science, Vietnam Academy of Science and Technology, 18 Hoang Quoc Viet Str., Cau Giay Distr., Hanoi, Vietnam. E-mail: trinhpv@ims.vast.vn; thangbh@ims.vast.ac.vn; chucnv@ims.vast.vn; Tel: +84 943190301*

[b]*Graduate University of Science and Technology, Vietnam Academy of Science and, Technology, 18 Hoang Quoc Viet Str., Cau Giay Distr., Hanoi, Vietnam*

[c]*Institute of Sciences and Technology, TNU – University of Sciences, Tan Thinh Ward, Thai Nguyen City, Vietnam*

[d]*Center for High Technology Research and Development, Vietnam Academy of Science and Technology, 18 Hoang Quoc Viet Str., Cau Giay Distr., Hanoi, Vietnam*

Table 1 The previous studies on the thermal conductivity of ternary hybrid nanofluids

Ref.	Nanoadditives	Base fluid	Concentration	Temperature	Conductivity enhancement
Cakmak *et al.*,[21]	rGO–Fe_3O_4–TiO_2	EG	0.1–0.25 wt%	25–60 °C	Up to 13.3%
Boroomandpour *et al.*,[22]	MWCNTs–TiO_2–ZnO	Water–EG	0.1–0.45 vol%	25–50 °C	Up to 18.7%
Ahmed *et al.*,[23]	ZnO–Al_2O_3–TiO_2	Water	0.025–0.1 vol%	20–50 °C	Up to 69%
Dezfulizadeh *et al.*,[24]	Cu–SiO_2–MWCNTs	Water	1–3 vol%	15–65 °C	40–80%
Esfe *et al.*,[25]	SWCNT–TiO_2–CuO	Water	0.05–1.65%	26–50 °C	Up to 34%
Esfe *et al.*,[26]	SWCNT–Fe_3O_4–CuO	Water–EG	0.03–0.94%	26–50 °C	29–39.2%
Trinh *et al.*,[27]	Gr–CNT–CuNP	EG	0.005–0.035 vol%	30–60 °C	10–41%
Baby *et al.*,[28]	MWNT–Gr–AgNP	EG	0.005–0.04 vol%	25–50 °C	1–20%
This work	Gr–CNT–AgNP	EG	0–0.05 vol%	30–55 °C	Up to 52%
		Water	0–0.05 vol%	30–55 °C	Up to 38%

synergistically improve thermophysical properties beyond what can be achieved with single- or dual-component systems. Several studies have demonstrated the advantages of THFs, including enhanced thermal conductivity, improved rheological behavior, and broader application potential.[17,19,20] The summary of recent works related to the thermal properties of the THFs was listed in Table 1.

Recent investigations provide compelling evidence of the efficiency of THFs. Cakmak *et al.* reported a 13.3% conductivity enhancement in rGO/Fe_3O_4/TiO_2-based THFs at 0.25 wt%.[21] The comparative analysis of the thermal conductivity of THFs containing rGO/Fe_3O_4/TiO_2 and found that the thermal conductivity enhancement of THFs is higher than that of mono nanofluids containing single nanoadditives like TiO_2, GNP, Fe_2O_3, Fe_3O_4, and hybrid nanofluids containing rGO–TiO_2, rGO–GO.[29–32] Boroomandpour and coworkers achieved an 18.7% enhancement in MWCNT–TiO_2–ZnO THFs with 0.4 wt% loading.[22] Even higher improvements have been reported: Ahmed *et al.*[23] observed a 69% enhancement in Al_2O_3–TiO_2–ZnO THFs at 0.1 vol%, while Dezfulizadeh *et al.*.[24] recorded an 80% increase in Cu–SiO_2–MWCNT THFs at 65 °C and 3 wt% additive concentration. Esfe and coworkers also demonstrated notable enhancements in THFs containing combinations such as SWCNT–TiO_2–CuO and SWCNT–Fe_3O_4–CuO.[25,26] More recently, hybrid materials that combine graphene and CNTs with metallic nanoparticles—including Cu and Ag—have gained interest due to their ability to exploit complementary thermal conduction mechanisms.[27,28] These hybrid structures offer improved interfacial contact, enhanced electron and phonon transport, and reduced thermal resistance within the fluid. Trinh *et al.* synthesized nanofluids containing Gr–MWCNT/CuNP hybrids and reported a thermal conductivity increase of up to 41%.[27,28] Baby *et al.* prepared MWCNT–HEG/AgNP-based nanofluids, achieving a 20% enhancement.[28] However, the enhancement in thermal conductivity was only about 20%, which was lower than expected. This limitation may be attributed to the use of graphene oxide (GO), whose thermal conductivity is reduced due to the presence of functional groups and structural defects formed during the preparation process. These findings highlight that the performance of THFs is strongly dependent on the structure, purity, and synergy of the incorporated nanoadditives. Therefore, designing hybrid materials with tailored architectures and optimized thermal transport pathways is essential for achieving next-generation heat-transfer fluids with superior performance.

Therefore, the primary objective of this study was to experimentally investigate the thermal conductivity of ternary hybrid nanofluids (THFs) containing Gr–CNT–AgNPs and to systematically evaluate the effects of nanoparticle concentration and temperature within a practically relevant operating range. An additional objective was to develop an accurate empirical correlation for predicting the thermal conductivity of these ternary hybrid nanofluids.

2 Materials and method

2.1. Materials

Lab-made MWCNTs (purity > 98%, 10–30 nm in diameter and 5–15 μm in length) (Fig. 1a) and graphene (purity > 99%, 3–8 nm in thickness and 0.5–1.5 μm in length) (Fig. 1b) were used for preparing the hybrid material.[33] Siver nitrate ($AgNO_3$) with a purity of 99% was provided by Sigma-Aldrich. Other chemicals including HNO_3, H_2SO_4, NaOH and $NaBH_4$ were supplied by Xilong Chemical Co. Ltd.

2.2. Preparation of ternary hybrid nanofluids

The fabrication process of ternary hybrid nanofluid containing Gr–CNT–AgNP hybrid materials is presented in Fig. 2. Firstly, Gr and CNTs were modified with –COOH groups. 100 mg Gr was added in a mixture of 50 ml HNO_3 (65%) and 150 ml H_2SO_4 (98%) under continuous stirring (IKA C-MAG HS7 Hot Stirrer) of 300 rpm at 70 °C for 5 hours. After that, the acquired solutions were repeatedly filtered with deionized water until achieving a pH of approximately 7 to obtain Gr–COOH. CNT–COOH was also prepared by using the same process. A mixture of the prepared Gr–COOH and CNT–COOH with a weight ratio of 1 : 1 was dispersed together in ethylene glycol using bath ultrasonication (40 kHz, 150 W, Elmasonic S 30 H) for 30 minutes to produce a Gr–CNT solution. A specified volume of 0.05 M $AgNO_3$ solution was introduced into the Gr–CNT solution while maintaining continuous magnetic stirring with a speed of 300 rpm by an IKA C-MAG HS7 Hot Stirrer. The mixing process was kept for 30 minutes, then 20 ml of reducing solution containing NaOH and $NaBH_4$ (0.05 M) was dropped into the above

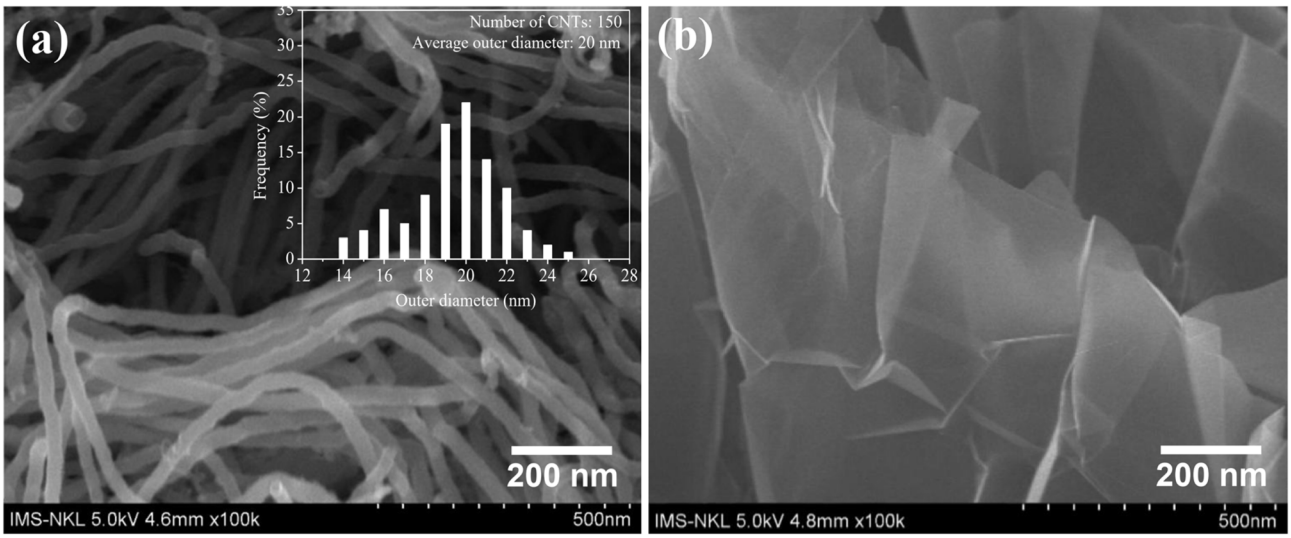

Fig. 1 SEM images of (a) CNTs and (b) graphene.

solution. The obtained solution was repeatedly filtered with deionized water and subsequently dried under vacuum at 60 °C for 24 hours to obtain Gr–CNT–AgNP hybrid materials. The calculated amounts of Gr–CNT–AgNP hybrid materials were dispersed in EG and DI water by bath ultrasonication (IKA C-MAG HS7 Hot Stirrer) for 30 min to prepare THFs with the concentrations of Gr–CNT–AgNP hybrid materials ranging from 0.001 to 0.005 vol%.

2.3. Instruments and characterization techniques

The microstructure of CNTs, Gr and Gr–CNT–AgNP hybrid materials was observed using FESEM (Hitachi S4800, Hitachi Ltd, Japan) with an accelerating voltage of 5 kV and TEM (JEOL JEM 2100, JEOL Ltd, Japan) with. The detail of the TEM sample preparation was described. A small amount of the sample (~0.1 mg) was dispersed in dispersed in dimethyl sulfoxide (DMSO) at low concentration and ultrasonicated for 15–20 min to ensure uniform dispersion and minimize agglomeration. A few microliters of the suspension were drop-cast onto carbon-coated copper TEM grids (300 mesh), which were pre-cleaned to improve wettability. Excess solvent was gently removed, and the grids were dried at room temperature. TEM observations were performed under an accelerating voltage of 200 kV. XRD

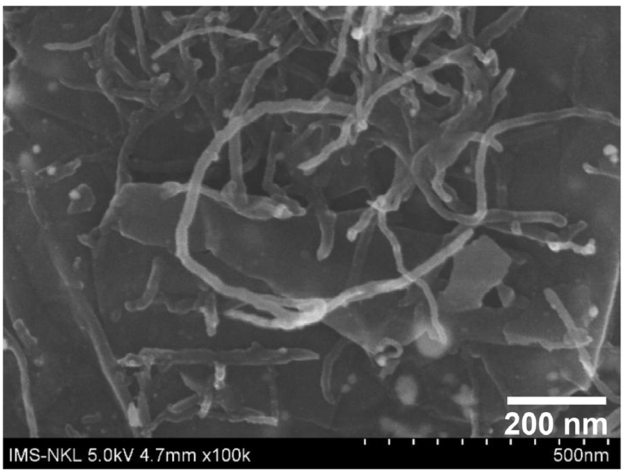

Fig. 3 SEM image of Gr–CNT–AgNP hybrid material.

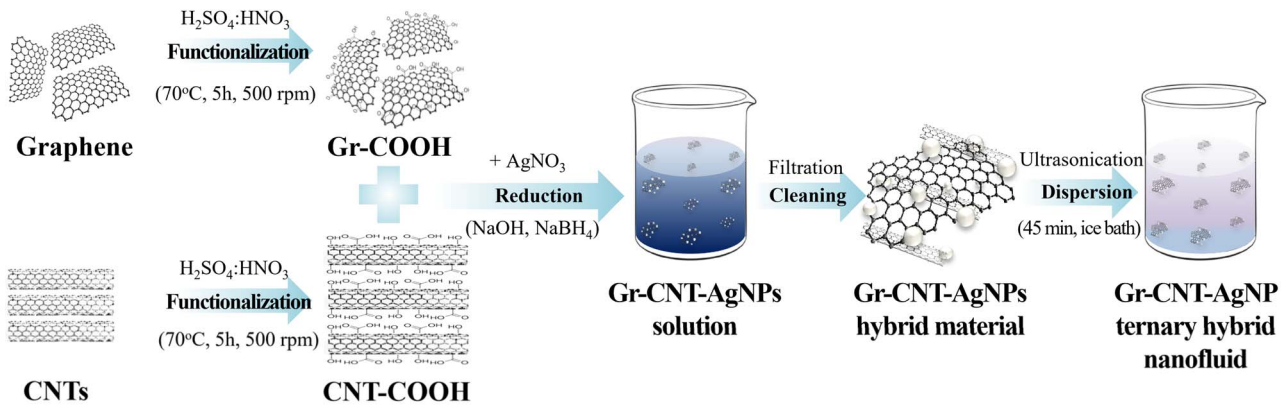

Fig. 2 Fabrication process of ternary hybrid nanofluid containing Gr–CNT–AgNPs.

patterns of samples were measured by using a D8 Endeavor (Bruker Corporation, Karlsruhe, Germany) with the radiation source of Cu-K_α at $\lambda = 1.54056$ Å. The samples were scanned between 10° and 80° degrees 2θ with step sizes of 0.01° and scan rate of 0.01° per second. The Shimadzu IR Prestige 21 (Shimadzu Corporation, Tokyo, Japan) spectrometer was employed to measure the FTIR spectra of the samples. The thermal conductivity of THFs in a range from 30 to 55 °C was measured using an HTL-04 system (Eternal Engineering Equipment Ltd, Maharashtra, India). The principle and measurement method for determining thermal conductivity using the HTL-04 device are described in detail in the SI. The reported results of the experiment are an average of five measurements for every nanofluid and the error bars in the figure mean standard deviation.

3 Results and discussion

3.1. Characterization of Gr–CNT–AgNP hybrid materials

Fig. 3 shows the FESEM image of Gr–CNT–AgNPs hybrid materials at high magnification. The results show that CNTs with an average diameter of around 20 nm and graphene sheets were intermixed, and the AgNPs with a diameter ranging from 2 nm to 16 nm were attached to CNTs and Gr surfaces. However, at a certain point, an AgNPs cluster was also observed due to small AgNPs agglomerating together to form larger clusters. The interlayer spacing of the nanoparticles was measured as shown in the TEM images at high magnification (Fig. 4). As a result, the spacing was approximately 0.235 nm, which is consistent with the standard interplanar spacing value $d_{(111)}$ of Ag nanoparticles[34] (Fig. 4c). Besides, the interlayer spacing of Gr and

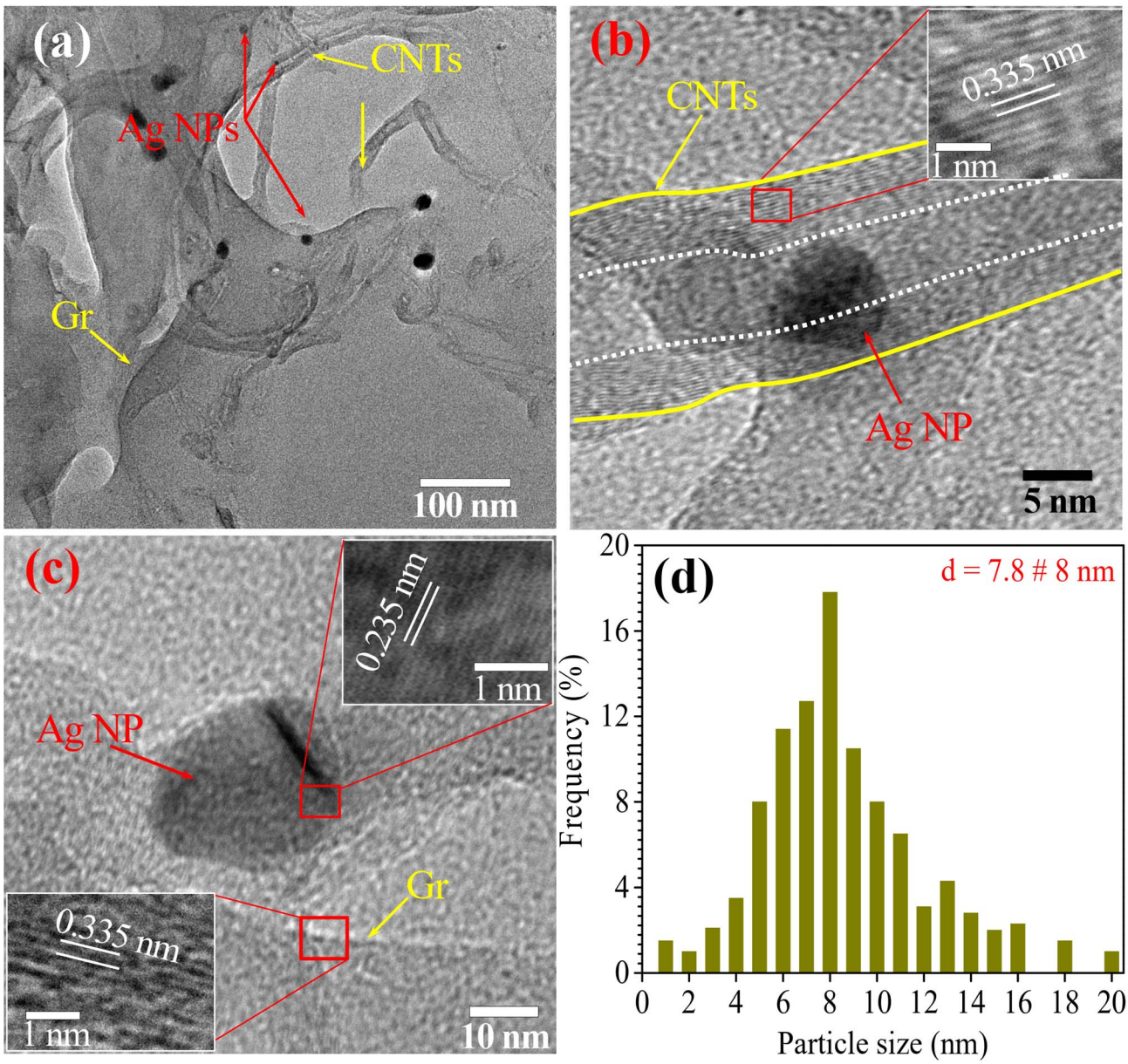

Fig. 4 (a–c) TEM images of Gr–CNT–AgNP hybrid material and (d) diameter distribution of AgNPs.

CNTs was also determined about 0.335 nm. This value is in good agreement with the reported works.[35,36] The distribution of AgNP size was determined by ImageJ software was shown in Fig. 4d. According to the diagram, the average diameter of AgNPs was calculated to be 8 nm. The FESEM and TEM image reveals a distribution and intercalation of MWNTs and AgNPs among the Gr sheets. These structure helps to minimize graphene layer restacking and enhances the effective surface area of the hybrid materials.[28]

Fig. 5 illustrates the XRD patterns of Gr–CNT and Gr–CNT–AgNPs hybrid materials. In the XRD pattern of Gr–CNT, the diffraction peak near 26.2°, 42° and 53.6° are attributed to the (002), (101), and (004) planes of hexagonal graphite, respectively originating from both graphene and CNTs.[37] For the XRD

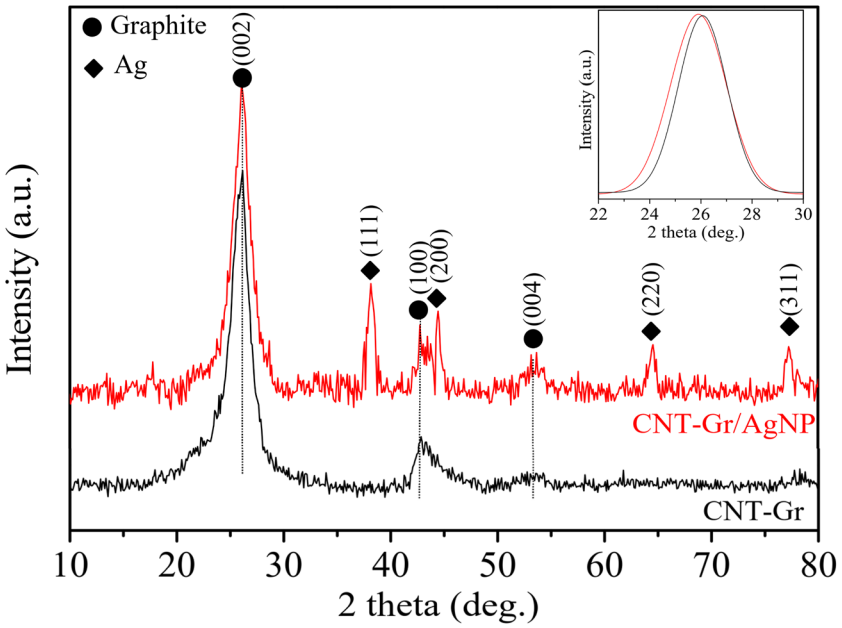

Fig. 5 XRD patterns of Gr–CNT and Gr–CNT–AgNPs hybrid materials.

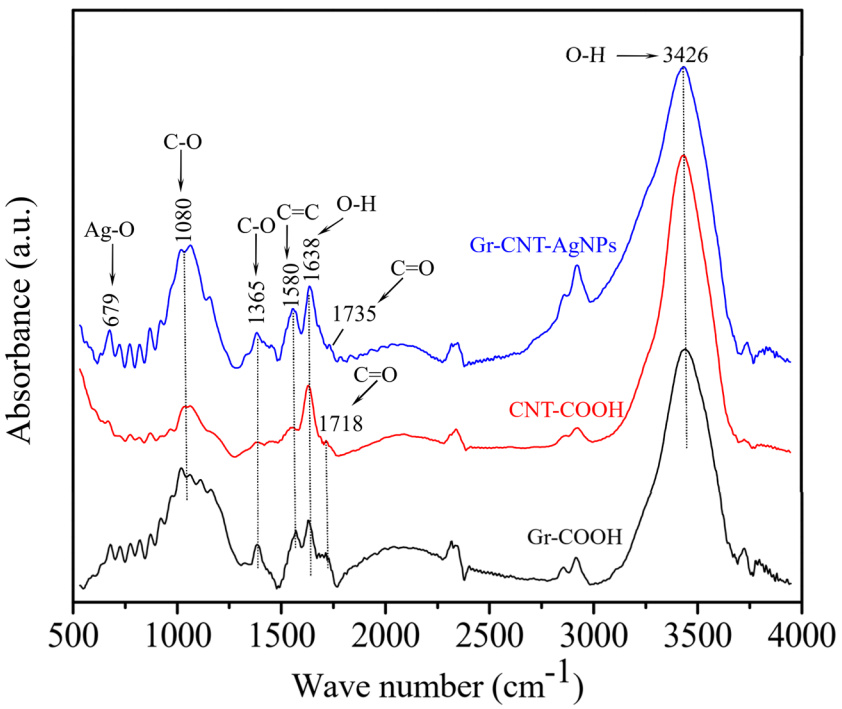

Fig. 6 FTIR spectra of Gr–COOH, CNT–COOH and Gr–CNT–AgNPs hybrid materials.

pattern of Gr–CNT–AgNPs hybrid materials, in addition to the characteristic peaks of Gr–CNT, new diffraction peaks are also observed. These typical peaks located at 38.2°, 44.3°, 64.2° and 77.5° corresponding to (111), (200), (220) and (311) planes of a face centered cubic crystal structure of Ag (JCPDS file no. 04-0783). The spacing $d_{(111)}$ of AgNPs has been calculated from the XRD pattern was 2.35 Å which is in good agreement with TEM results as discussed in the previous section. Besides, the crystallite size of AgNPs was estimated to be about 7 nm by using the Scherrer equation from the diffraction peaks. The full width at half maximum (FWHM) of the (002) peak corresponding to the graphite lattice of the samples was determined by using Gaussian fitting (insert image in Fig. 5). The obtained results showed that the FWHM of the (002) peak in the CNT–Gr/AgNPs material is larger than that of the CNT–Gr material. This may be attributed to the presence of metallic nanoparticles such as AgNPs, which can cause lattice distortion in both CNTs and Gr leading to increase of the interlayer spacing of graphite structure.[38,39] So, both XRD and morphology studies indicated that AgNPs were grown on the CNTs and Gr surfaces with a good size distribution and high crystallinity.

The FTIR studies were carried out to identify the presence of functional groups of the prepared samples as shown in Fig. 6. In the IR spectrum of Gr–COOH and CNT–COOH, the peaks observed at 1638 cm^{-1}, 1080 cm^{-1} and 1365 cm^{-1} could be assigned to characteristic stretch of carboxyl (–COOH) group, corresponding to stretching vibration of $\nu_{C=O}$, ν_{C-O} and ν_{C-OH} in carboxylic acid, respectively. The stretching vibration of the carbonyl ($\nu_{C=O}$) group was also attributed to the peak at 1718 cm^{-1}. The peak at 3426 cm^{-1} could be assigned to stretching vibrations of hydroxyl (O–H) groups.[40] While the IR spectra of Gr–CNT–AgNP hybrid materials showed the shift peaks from 1718 cm^{-1} to 1735 cm^{-1}, which corresponds to the band of carbonyl ($\nu_{C=O}$) group in ester, this is due to the esterification between the hydroxyl (–OH) and the carboxyl (–COOH) group of CNT–COOH and Gr–COOH. In addition, the peaks shift from 1080 cm^{-1} to 1064 cm^{-1}, and 1365 cm^{-1} to 1382 cm^{-1}, and 1638 cm^{-1} to 1635 cm^{-1}, and 3426 cm^{-1} to 3437 cm^{-1} and a new peak was observed at 679 cm^{-1}, which is assigned to the Ag–O stretching vibration.[41] Based on the peak shift in the functional groups and the appearance of a new Ag–O peak, suggesting that the silver ions attach to the hydroxyl and carboxyl groups, then after the complete reduction of the silver ions, the formation and growth of Ag nanoparticles promote the peaks shift in the functional groups.

The obtained results confirm that the formation of AgNPs follows the reduction pathway described in reaction (1). Specifically, when $NaBH_4$ is introduced into the $AgNO_3$ solution, it acts as a strong reducing agent, progressively converting Ag^+ ions into metallic silver nuclei. As the reaction proceeds, these nuclei grow and stabilize into well-defined Ag nanoparticles. During this process, the carboxyl functional groups generated on the surfaces of Gr sheets and CNTs play a crucial role. These groups not only promote strong interfacial interactions between AgNPs and the carbon nanomaterials but also provide active nucleation sites that facilitate the uniform deposition and anchoring of Ag nanoparticles onto the Gr and CNT structures (Fig. 7). This synergy contributes to the efficient formation and stable distribution of AgNPs within the hybrid material.

$$2AgNO_3 + NaBH_4 \rightarrow 2Ag + B_2H_6 + H_2 + 2NaNO_3 \quad (1)$$

3.2. Thermal conductivity of THFs

The thermal conductivity of the nanofluid was measured in the temperature range of 30–55 °C because this interval is commonly used in practical heat-transfer applications such as electronic cooling, heat exchangers, and solar-thermal systems.[42] Within this range, the nanofluid remains thermally and colloidally stable, thereby avoiding issues such as nanoparticle agglomeration, sedimentation, or base-fluid degradation that may occur at higher temperatures.[43,44] In addition, temperatures approaching the boiling point of the base fluid may introduce measurement uncertainties due to bubble formation, enhanced natural convection, and flow instability, which can adversely affect the accuracy of thermal conductivity measurements.[45,46] Therefore, the temperature range of 30–55 °C enables a clear observation of the temperature dependence of thermal conductivity while ensuring reliable and accurate measurements with the employed instrumentation. The thermal conductivity of THFs using distilled water as base fluid is presented in Fig. 8a. The obtained results indicated that the thermal conductivity of the THFs increases when increasing the

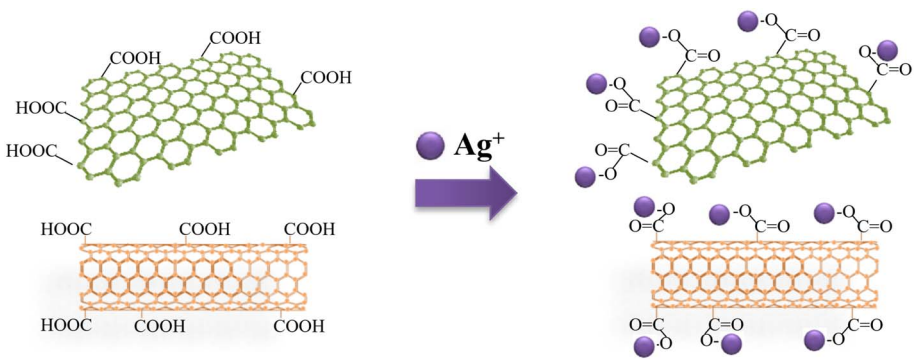

Fig. 7 Fomation of Gr–CNT–AgNP hybrid materials.

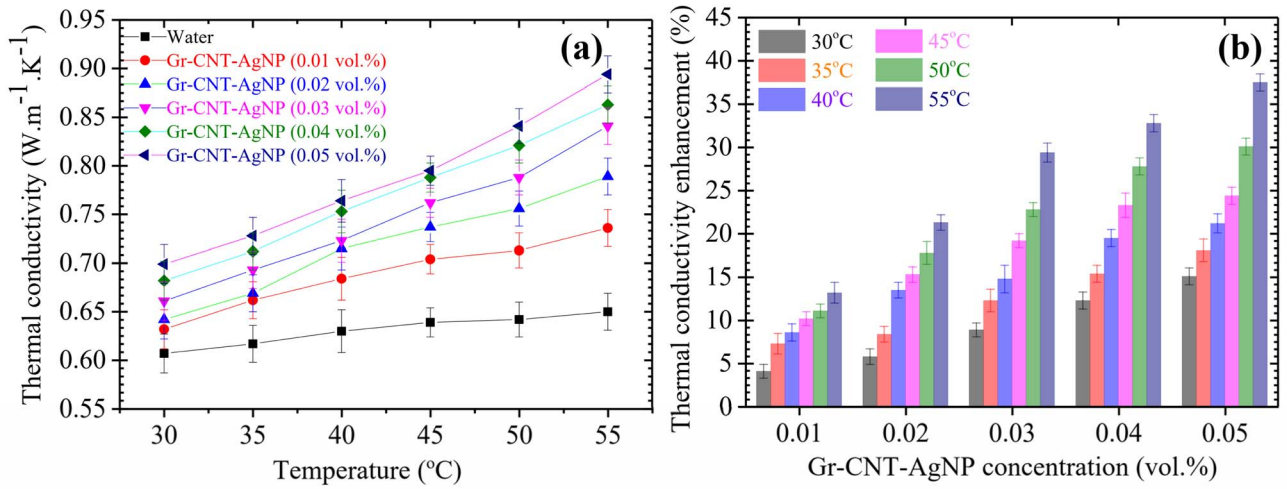

Fig. 8 (a) Thermal conductivity and (b) enhancement in thermal conductivity of water-based ternary hybrid nanofluid containing different Gr–CNT–AgNP concentrations. The error bars represent the standard deviation of the reported values.

Gr–CNT–AgNP concentrations. For example, at 30 °C, the thermal conductivity of the THFs containing 0.005% Gr–CNT–AgNP was measured to be 0.685 W m^{-1} K^{-1}, which is significantly higher than that of the distilled water (0.607 W m^{-1} K^{-1}). Fig. 8b and show the enhancement of the thermal conductivity of the water-based THFs. It can be seen, that the increase in thermal conductivity of the THFs is proportional to the increase in the concentration of Gr–CNT–AgNP hybrid materials and the measured temperatures. At 30 °C, the thermal conductivity enhancements of the THFs containing 0.001%, 0.002%, 0.003%, 0.004% and 0.005% were determined to be 4%, 6%, 9%, 13% and 15% respectively, higher than that of distilled water. It is noted that the increase in thermal conductivity of the nanofluid was considerably more pronounced when assessed at higher temperatures. Specifically, at the measurement temperature of 55 °C, the thermal conductivity enhancement of the THFs containing 0.005% Gr–CNT–AgNP was determined to be 37.6% higher than that of distilled water. It is noteworthy that the thermal conductivity ratio exhibits several outliers at 55 °C, which can be primarily attributed to the reduced colloidal stability of the nanofluid at elevated temperatures.[46–48] Increased thermal motion at elevated temperatures enhances Brownian collisions between nanoparticles, which can promote agglomeration and transient sedimentation, thereby leading to increased scatter in the measured thermal conductivity data.[46] At higher temperatures, enhanced Brownian motion and weakened intermolecular interactions can promote partial nanoparticle agglomeration or sedimentation, which leads to temporary fluctuations in the local particle concentration.[49] These fluctuations may cause instability in the signal and result

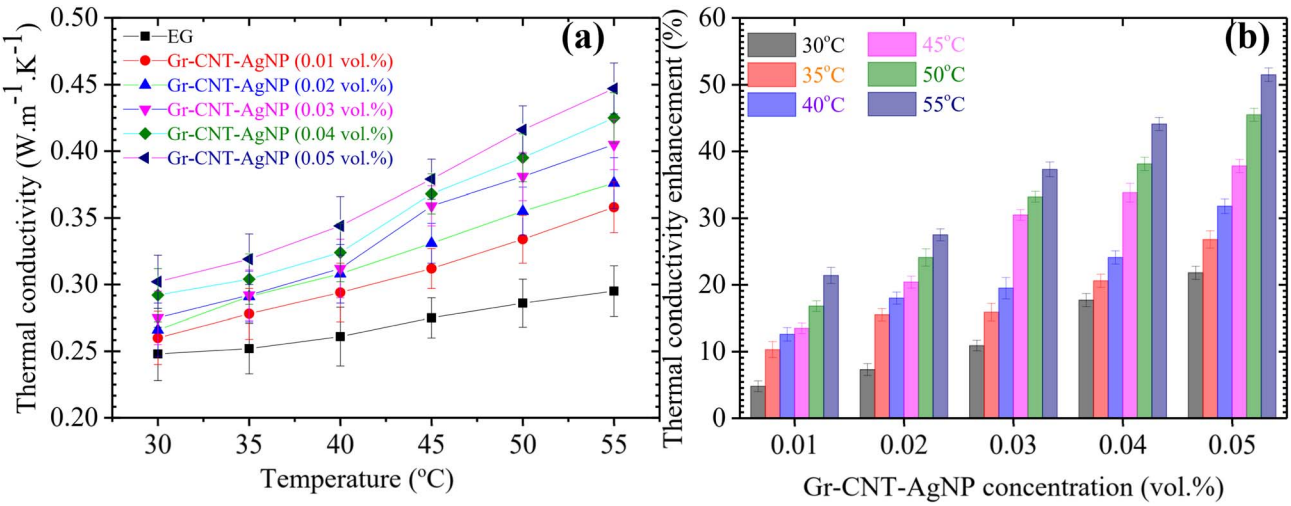

Fig. 9 (a) Thermal conductivity and (b) enhancement in thermal conductivity of EG-based ternary hybrid nanofluid containing different Gr–CNT–AgNP concentrations. The error bars represent the standard deviation of the reported values.

in scattered data points. Additionally, higher temperatures may increase natural convection effects in the measuring cell, further contributing to outliers at 55 °C.[49–51]

Fig. 9a shows the influence of the Gr–CNT–AgNP concentrations on the thermal conductivity of EG-based THFs. Similarly to water-based THFs, the thermal conductivity of EG-based THFs increases when the concentration of Gr–CNT–AgNP hybrid materials increases. The nanofluid containing Gr–CNT–AgNP exhibits the thermal conductivity enhancement of 5%, 7%, 11%, 18% and 22% with 0.001%, 0.002%, 0.003%, 0.004% and 0.005% Gr–CNT–AgNP, respectively (Fig. 9b). The thermal conductivity enhancement of THFs could be explained according to Sastry *et al.*[52] CNTs act as thermal bridges to connect the network and help to avoid Gr stacking. Graphene sheets form an interconnected network (as shown in SEM and TEM images), leading to better enhancement in heat transfer.[53] In addition, the presence of AgNPs with high thermal conductivity helps to avoid the Gr stacking and expand the overall surface area.[54] The thermal conductivity of THFs was augmented when assessed at higher temperatures. The highest thermal conductivity enhancement was determined to be 52% compared to EG for THFs containing 0.005 vol% Gr–CNT–AgNP. The obtained results show certain agreement with previously published studies on ternary hybrid nanofluids Table 1. The prepared THFs exhibited higher improvement compared to the THFs containing MWNT–HEG/AgNPs reported by Baby *et al.*[28] This could be due to the bond between Gr, CNTs and Ag improved *via* the interaction between Ag^+ ion and the functional groups attached to Gr, CNTs surface. The improvement in interface bond strength between Ag and Gr, CNTs lead to enhance the electron and phonon transfer and thus improve the thermal conductivity of the nanofluids. The improvement in the thermal conductivity of THFs at higher concentrations can be attributed to the percolation effect, which reduces the mean free path of nanoparticles or increases their volume fraction, thereby intensifying lattice vibrations.[55] Li *et al.* further identified Brownian motion, particle agglomeration, and viscosity as key factors influencing the temperature-dependent thermal conductivity of nanofluids.[56] According to their findings, an increase in temperature produces two main effects: (i) a reduction in nanoparticle cluster formation and (ii) enhanced Brownian motion. Together, these phenomena contribute to the observed increase in the thermal conductivity of THFs with rising temperature.

The correlation between the thermal conductivity (K) of THFs and the concentration of Gr–CNT–AgNP hybrid material could be expressed using a linear function as the following:[57]

$$\frac{K_{\mathrm{THF}}}{K_{\mathrm{bf}}} = 1 + \alpha \times \varphi \tag{2}$$

where K_{THF} and K_{bf} represent the thermal conductivities of the THFs and base fluid, respectively. These values are influenced by the concentration (φ) of Gr–CNT–AgNP hybrid materials. The factor α is a numerical coefficient associated with the measured temperatures. The value of α factor for both water-based and EG-based ternary hybrid nanofluids was estimated by using Origin Pro 9 as shown in Fig. 10. The estimated values of α factor are displayed in Table 2, indicating an R^2 superior to

Table 2 The value of α factor was estimated by using linear fitting of the thermal conductivity *versus* Gr–CNT–AgNP concentrations

Concentrations (vol%)	Water-based ternary hybrid nanofluids		EG-based ternary hybrid nanofluids	
	α	R^2	α	R^2
0	3.14×10^{-4}	0.99998	4.21×10^{-4}	0.99996
0.001	4.26×10^{-4}	0.99976	5.33×10^{-4}	0.99937
0.002	4.51×10^{-4}	0.99942	6.79×10^{-4}	0.99905
0.003	5.61×10^{-4}	0.99915	7.66×10^{-4}	0.99891
0.004	6.43×10^{-4}	0.99931	8.49×10^{-4}	0.99882
0.005	8.41×10^{-4}	0.99891	11.10×10^{-4}	0.99812

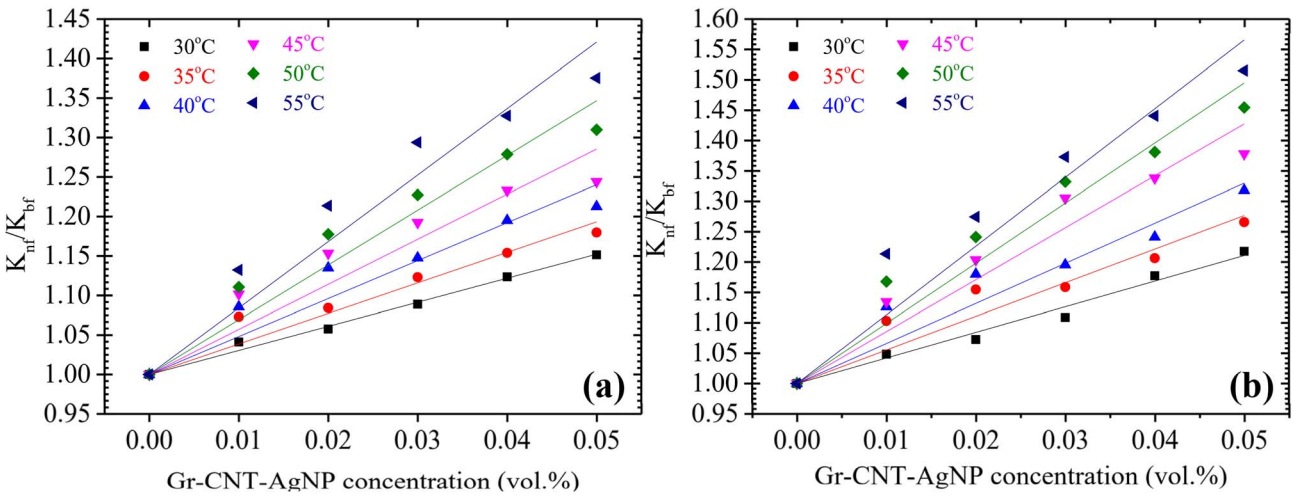

Fig. 10 Thermal conductivity ratio of the ternary hybrid nanofluids *versus* different measured temperatures (a) water-based and (b) EG-based ternary hybrid nanofluids.

Table 3 Values of factors (*A*, *B*, *C*, *D*, *E*) of the eqn (3) estimated by using Poly4-FitFunc of α values for water-based and EG-based ternary hybrid nanofluids

	Water-based ternary hybrid nanofluids	EG-based ternary hybrid nanofluids
Factors	$R^2 = 0.96643$	$R^2 = 0.99998$
A	−0.00581	0.02285
B	5.17606×10^{-4}	−0.00236
C	-1.58711×10^{-5}	9.04064×10^{-5}
D	2.08741×10^{-7}	-1.50337×10^{-6}
E	-9.33333×10^{-10}	9.23333×10^{-9}

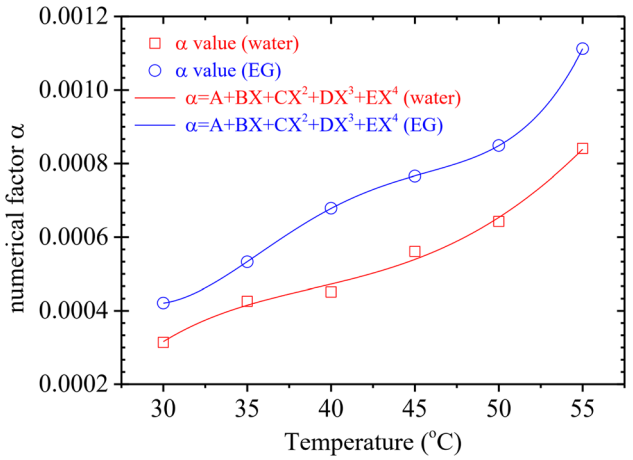

Fig. 11 Values of fitting parameter α using Poly4-FitFunc for water-based and EG-based ternary hybrid nanofluids.

0.99. Furthermore, the thermal conductivity of the produced THFs elevated as assessed at higher temperatures. The thermal conductivity enhancement has a nearly linear relationship with the concentration of Gr–CNT–AgNP hybrid materials and a nonlinear relationship with the measured temperatures. Therefore, it could be articulated by a quartic polynomial function relationship:[58]

$$\alpha = A + B \times X + C \times X^2 + D \times X^3 + E \times X^4 \quad (3)$$

where *A*, *B*, *C*, *D* and *E* are numerical factors. The relationship between α and temperature *X*, along with eqn (3), was shown in Fig. 11. By integrating eqn (2) and (3), a general relationship of the $\frac{K_{THF}}{K_{bf}}$ ratio for Gr–CNT–AgNP concentration and temperature can be given as the following eqn (4):

$$\frac{K_{THF}}{K_{bf}} = 1 + A \times \varphi + B \times X \times \varphi + C \times X^2 \times \varphi + D \times X^3 \times \varphi + E \times X^4 \times \varphi \quad (4)$$

By using Poly4-FitFunc of OriginPro 9, the values of factors (*A*, *B*, *C*, *D*, *E*) of eqn (2) were estimated for water-based and EG-based THFs as presented in Table 3. The fitting results are shown as a graph in Fig. 12, which demonstrates that the experimental data matched smoothly with the proposed eqn (3). The obtained results indicated that, in addition to factors such as conductivity and the concentration of nanoadditives, the influence of measured temperature on thermal conductivity of nanofluid cannot be neglected. This dependence is represented by factor α, a fourth-order polynomial function *via* eqn (3). The

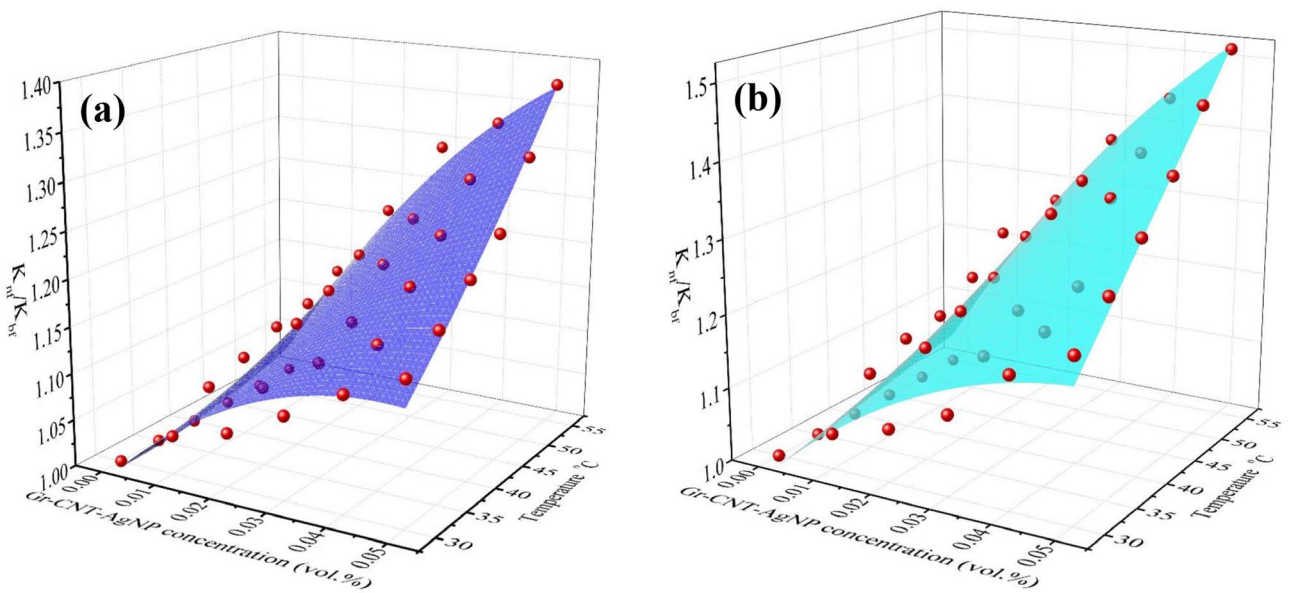

Fig. 12 Thermal conductivity ratio of ternary hybrid nanofluids *versus* Gr–CNT–AgNP concentrations and temperatures (a) water-based and (b) EG-based ternary hybrid nanofluids. The points represent experimental values, whereas the surfaces are derived from the fitting function (3).

proposed model enables researchers to more accurately evaluate the thermal conductivity of nanofluids.

4 Conclusion

The thermal conductivity of ternary hybrid nanofluids containing Gr–CNT–AgNPs was experimentally investigated. The influences of nanoparticle concentration and temperature were systematically evaluated. The results showed that increasing the Gr–CNT–AgNPs concentration significantly improved the thermal conductivity of both base fluids. At a loading of 0.05 vol%, the maximum thermal conductivity enhancement reached 38% for water-based nanofluid and 52% for EG-based nanofluid, respectively. In addition to concentration, temperature also played a notable role, as the intensified Brownian motion at elevated temperatures further contributed to the enhancement in thermal conductivity. The proposed correlation based on a quartic polynomial function relationship exhibited strong agreement with the experimental data with R^2 of 0.96643 and 0.99998 for water-based THFs and EG-based THFs, respectively, confirming the accuracy and reliability of the model for the prediction of the thermal conductivity of ternary hybrid nanofluids.

Nevertheless, this study has certain limitations that should be acknowledged. The experimental investigation was limited to a moderate temperature range (30–55 °C), selected to ensure measurement reliability and colloidal stability; therefore, the behavior of the nanofluids at higher temperatures, where instability and convection effects may become more pronounced, was not examined. In addition, thermal conductivity measurements were performed under controlled laboratory conditions, and the influence of flow, shear, and long-term operation on nanofluid stability was not addressed. Minor data scatter observed at the upper temperature limit further suggests that colloidal stability may be reduced at elevated temperatures.

Future research should extend the temperature range and evaluate the long-term stability and thermophysical performance of Gr–CNT–AgNPs nanofluids under dynamic flow conditions relevant to practical systems. Further studies should also focus on validating the proposed correlation under different operating conditions and exploring the application of these nanofluids in realistic thermal systems such as electronic cooling devices, heat exchangers, and internal combustion engines.

Author contributions

Pham Van Trinh: conceptualization, methodology, investigation, formal analysis, writing – original draft preparation, writing – reviewing and editing. Nguyen Ngoc Anh: conceptualization, methodology, investigation. Mai Thi Phuong: formal analysis, investigation. Nguyen Van Tu: formal analysis, investigation. Tran Van Hau: formal analysis, investigation. Do Tuan: formal analysis, investigation. Nguyen Thi Huyen: formal analysis, investigation. Cao Thi Thanh: formal analysis, investigation. Nguyen Van Hao: formal analysis, investigation. Mone Phommahaxay: formal analysis, investigation. Nguyen Thi Ngoc Mai: investigation. Phan Ngoc Hong: formal analysis, investigation. Phan Ngoc Minh: supervision, writing – original draft preparation, writing – reviewing and editing. Bui Hung Thang: conceptualization, writing – reviewing and editing. Nguyen Van Chuc: conceptualization, project administration, writing – reviewing and editing. All authors discussed and approved the manuscript.

Conflicts of interest

The authors declare no possible conflict of interests.

Abbreviations

Gr	Graphene
GNP	Graphene nanoplateletes
CNTs	Carbon nanotubes
MWCNTs	Multiwalled carbon nanotubes
SWCNTs	Single walled carbon nanotubes
Gr–CNT	Graphene–carbon nanotube hybrid material
CuNPs	Copper nanoparticles
AgNPs	Silver nanoparticles
Gr–CNT–AgNPs	Graphene–carbon nanotube–silver nanoparticles
DI	Deionized
EG	Ethylene glycol
THF	Ternary hybrid nanofluids
FESEM	Field emission scanning electron mircoscopy
TEM	Transmission electron mircoscopy
FTIR	Fourier transform infrared spectroscopy
K_{THF}	Thermal conductivity of ternary hybrid nanofluids [W m^{-1} K^{-1}]
K_{bf}	Thermal conductivity of base fluid [W m^{-1} K^{-1}]
K_{THF}/K_{bf}	Thermal conductivity ratio
A, B, C, D, E	Eqn (2) numerical factors
α	A numerical coefficient associated with the measured temperatures
φ	Volume concentration [vol%]
X	Temperature [°C]

Data availability

The authors confirm that the data supporting the findings of this study are available within the articles. Raw data that support the findings of this study are available from the corresponding author, upon reasonable request.

Supplementary information (SI) is available. See DOI: https://doi.org/10.1039/d5ra03763h.

Acknowledgements

This research was funded by the Vietnam Academy of Science and Technology (VAST) under Project NCXS02.03/24-25.

References

1 W. Yao, G. Zhu, Z. Yan, W. Tong and D. Fan, *Appl. Mater. Today*, 2025, **44**, 102719.

2 H. Chen, T. Zhang, Q. Gao, J. Lv, H. Chen and H. Huang, *Energy*, 2025, **316**, 134575.
3 M. A. Rahman, S. M. M. Hasnain, S. Pandey, A. Tapalova, N. Akylbekov and R. Zairov, *ACS Omega*, 2024, **9**(30), 32328–32349.
4 H. B. Bacha, N. Ullah, A. Hamid and N. A. Shah, *Int. J. Thermofluids*, 2024, **22**, 100595.
5 V. Nair, A. D. Parekh and P. R. Tailor, *J. Braz. Soc. Mech. Sci. Eng.*, 2018, **40**, 1–17.
6 F. S. Alkasmoul, M. T. Al-Asadi, T. G. Myers, H. M. Thompson and M. C. T. Wilson, *Int. J. Heat Mass Tran.*, 2018, **126**, 639–651.
7 V. Ghazanfari, A. Taheri, Y. Amini and F. Mansourzade, *Case Stud. Therm. Eng.*, 2024, **53**, 103864.
8 S. Kumar and R. Kumar, *Wear*, 2023, **518–519**, 204623.
9 N. Van Hao, D. H. Tung, T. T. Thao, V. X. Hoa, N. H. Thoan, P. T. Tan, P. N. Minh, J. Fal, G. Żyła and P. Van Trinh, *J. Therm. Anal. Calorim.*, 2023, **148**, 7579–7590.
10 O. A. Hussein, M. H. Rajab, O. A. Alawi, M. W. Falah, A. H. Abdelrazek, W. Ahmed, M. Eltaweel, R. Z. Homod and Z. M. Yaseen, *Appl. Therm. Eng.*, 2023, **229**, 120545.
11 G. Bharadwaj, K. Sharma, A. K. Pandey and A. Gupta, *J. Therm. Anal. Calorim.*, 2024, **149**(5), 1859–1893.
12 M. H. Esfe, D. Toghraie and M. S. Karajabad, *J. Therm. Anal. Calorim.*, 2025, **150**(12), 9255–9264.
13 R. Sadri, G. Ahmadi, H. Togun, M. Dahari, S. N. Kazi, E. Sadeghinezhad and N. Zubir, *Nanoscale Res. Lett.*, 2014, **9**, 1–16.
14 H. Yarmand, S. Gharehkhani, G. Ahmadi, S. F. S. Shirazi, S. Baradaran, E. Montazer, M. N. M. Zubir, M. S. Alehashem, S. N. Kazi and M. Dahari, *Energy Convers. Manag.*, 2015, **100**, 419–428.
15 S. S. J. Aravind and S. Ramaprabhu, *RSC Adv.*, 2013, **3**, 4199–4206.
16 W. A. Khan, S. N. Kazi, Z. Z. Chowdhury, M. N. M. Zubir, Y. H. Wong, K. Shaikh and R. Nawaz, *Sol. Energy Mater. Sol. Cells*, 2024, **276**, 113046.
17 M. I. I. Rabby, M. W. Uddin, N. M. S. Hassan, M. Al Nur, R. Uddin, S. Istiaque and M. M. M. Abir, *J. Mol. Liq.*, 2024, **408**, 125257.
18 P. Priyadharshini, M. V. Archana, N. A. Shah and M. H. Alshehri, *Symmetry*, 2023, **15**, 1225.
19 H. Adun, D. Kavaz and M. Dagbasi, *J. Clean. Prod.*, 2021, **328**, 129525.
20 R. Aalikhani, D. Toghraie, B. Mehmandoust and S. Salahshour, *Results Eng.*, 2025, **26**, 105295.
21 N. K. Cakmak, Z. Said, L. S. Sundar, Z. M. Ali and A. K. Tiwari, *Powder Technol.*, 2020, **372**, 235–245.
22 A. Boroomandpour, D. Toghraie and M. Hashemian, *Synth. Met.*, 2020, **268**, 116501.
23 W. Ahmed, S. N. Kazi, Z. Z. Chowdhury, M. R. B. Johan, S. Mehmood, M. E. M. Soudagar, M. A. Mujtaba, M. Gul and M. S. Ahmad, *Renew. Sustain. Energy Rev.*, 2021, **145**, 111025.
24 A. Dezfulizadeh, A. Aghaei, A. H. Joshaghani and M. M. Najafizadeh, *Powder Technol.*, 2021, **389**, 215–234.
25 M. H. Esfe, S. Alidoust, D. Toghraie and H. Hatami, *J. Therm. Anal. Calorim.*, 2025, **150**(6), 4177–4189.
26 M. H. Esfe, H. Hatami, S. Alidoust, D. Toghraie and M. S. Karajabad, *J. Therm. Anal. Calorim.*, 2024, **149**(14), 7773–7781.
27 P. Van Trinh, N. N. Anh, B. H. Thang, L. D. Quang, N. T. Hong, N. M. Hong, P. H. Khoi, P. N. Minh and P. N. Hong, *RSC Adv.*, 2016, **7**, 318–326.
28 T. T. Baby and R. Sundara, *AIP Adv.*, 2013, **3**, 12111.
29 M. M. Heyhat, S. Kimiagar, N. G. S. G. Abad and E. Feyzi, *Phys. Chem. Res.*, 2016, **4**, 407–415.
30 A. Moghadassi, E. Ghomi and F. Parvizian, *Int. J. Therm. Sci.*, 2015, **92**, 50–57.
31 D. H. Yoo, K. S. Hong and H. S. Yang, *Thermochim. Acta*, 2007, **455**, 66–69.
32 N. Kumar and S. S. Sonawane, *Int. Commun. Heat Mass Tran.*, 2016, **78**, 277–284.
33 P. Van Trinh, N. N. Anh, N. T. Hong, P. N. Hong, P. N. Minh and B. H. Thang, *J. Mol. Liq.*, 2018, **269**, 344–353.
34 A. J. Kora, S. R. Beedu and A. Jayaraman, *Org. Med. Chem. Lett.*, 2012, **2**, 1–10.
35 B. Wang, Q. Y. Chang and K. Gao, *Appl. Surf. Sci.*, 2019, **479**, 20–24.
36 O. V. Kharissova and B. I. Kharisov, *RSC Adv.*, 2014, **4**, 30807–30815.
37 T. T. Baby and S. Ramaprabhu, *Nanoscale*, 2011, **3**, 2208–2214.
38 G. F. Liu, L. J. Huang, Y. X. Wang, J. G. Tang, Y. Wang, M. M. Cheng, Y. Zhang, M. J. Kipper, L. A. Belfiore and W. S. Ranil, *RSC Adv.*, 2017, **7**, 49159–49165.
39 D. Lin, L. A. Diaz-Torres, M. Băjan, D. L. Cursaru and S. Mihai, *Membranes*, 2025, **15**, 158.
40 Y. Si and E. T. Samulski, *Nano Lett.*, 2008, **8**, 1679–1682.
41 P. J. G. Goulet and R. F. Aroca, *Can. J. Chem.*, 2004, **82**, 987–997.
42 F. Rubbi, L. Das, K. Habib, N. Aslfattahi, R. Saidur and M. T. Rahman, *Sol. Energy Mater. Sol. Cells*, 2021, **230**, 111220.
43 S. Chakraborty and P. K. Panigrahi, *Appl. Therm. Eng.*, 2020, **174**, 115259.
44 B. Mehta, D. Subhedar, H. Panchal and Z. Said, *J. Mol. Liq.*, 2022, **364**, 120034.
45 E. V. Timofeeva, J. L. Routbort and D. Singh, *J. Appl. Phys.*, 2009, **106**, 014304.
46 S. K. Das, N. Putra, P. Thiesen and W. Roetzel, *J. Heat Transfer*, 2003, **125**, 567–574.
47 A. Moradi, M. Zareh, M. Afrand and M. Khayat, *Powder Technol.*, 2020, **362**, 578–585.
48 A. Borode, T. Tshephe, P. Olubambi, M. Sharifpur and J. Meyer, *J. Therm. Anal. Calorim.*, 2024, **149**(10), 5059–5083.
49 R. Azizian, E. Doroodchi and B. Moghtaderi, *Ind. Eng. Chem. Res.*, 2011, **51**, 1782–1789.
50 T. Islam, M. N. Alam, S. Niazai, I. Khan, M. Fayz-Al-Asad and S. Alqahtani, *Sci. Rep.*, 2023, **13**(1), 21171.
51 L. Wang, B. Shi and Z. Chai, *Appl. Therm. Eng.*, 2018, **128**, 204–213.

52 N. N. V. Sastry, A. Bhunia, T. Sundararajan and S. K. Das, *Nanotechnology*, 2008, **19**, 055704.
53 J. Koo, Y. Kang and C. Kleinstreuer, *Nanotechnology*, 2008, **19**, 375705.
54 J. J. Wang, R. T. Zheng, J. W. Gao and G. Chen, *Nano Today*, 2012, **7**, 124–136.
55 T. T. Baby and R. Sundara, *J. Phys. Chem. C*, 2011, **115**, 8527–8533.
56 Y. H. Li, W. Qu and J. C. Feng, *Chin. Phys. Lett.*, 2008, **25**, 3319.
57 C. Nolan and S. Herbert, *Math. Educ. Res. J.*, 2015, **27**(4), 401–421.
58 P. Bhattacharyya and Y. E. Arumaraj, *Ann. Fenn. Math.*, 1981, **6**, 197–203.